13th IEA Heat Pump Conference 2020

13th IEA Heat Pump Conference
April 26-29, 2021 Jeju, Korea

Experimental and Mechanistic Numerical Analysis of a Variable Speed Residential Heat Pump Unit with an Expansion Work-Recovery Device

Riley B. Barta[a,*], Ammar M. Bahman[a,b], Lennart Stania[a], Davide Ziviani[a], Eckhard A. Groll[a]

[a]Ray W. Herrick Laboratories, School of Mechanical Engineering, Purdue University
West Lafayette, 47907-2099, USA
bartar@purdue.edu; abahman@purdue.edu; stania@tfd.uni-hannover.de; dziviani@purdue.edu; groll@purdue.edu
[b]Mechanical Engineering Department, College of Engineering and Petroleum, Kuwait University
P.O. Box 5969, Safat 13060, Kuwait
a.bahman@ku.edu.kw

Abstract

In recent years, variable-speed heat pump systems for residential applications have gained significant attention in order to improve the part-load operations during heating and cooling seasons. A single-stage 5-ton (17.58 kW) heat pump unit with R-410A as a working fluid has been considered as a test case to assess the performance of a variable-speed rolling piston compressor. Moreover, the heat pump has been retrofitted with a prototype expansion work-recovery device to replace the conventional expansion valve for cooling mode. The heat pump performance has been tested extensively in a pair of psychrometric chambers. In order to facilitate future optimization of the system, a fully-mechanistic steady-state cycle model of the heat pump has been developed. In particular, the system model is based on a charge-sensitive approach with semi-empirical models for the compressor and the work-recovery device as well as detailed heat exchanger models. The cycle model has been validated and tuned with the experimental data collected. Future work is to utilize the validated mechanistic model for cycle optimization and charge sensitivity studies.

Keywords: Variable speed; Expansion work recovery; Mechanistic model; Charge sensitive

1. Introduction

Growing concerns over climate change are driving innovation in almost every industry. However, given that in 2017, 38% of US energy consumption was in buildings [1], much of which is attributable to heating, ventilation, air conditioning, and refrigeration (HVAC&R), innovation in this industry is particularly vital. To this end, both academia and industry have been investigating different ways to increase the efficiency of the vapor compression cycle (VCC). Most of the optimization efforts focused on three of the four primary components in a VCC, being the compressor, the condenser, and the evaporator. Within these efforts, the use of variable-speed compressors represents a significant performance benefit without any fundamental changes to the cycle. The fourth component of a VCC enables the expansion from condensing to evaporating pressure and is generally achieved with a thermostatic expansion valve (TXV) or an electronic expansion valve (EXV). When modeling these devices an isenthalpic assumption is generally made, meaning that any potentially recoverable work from the expansion process is wasted. In response to this, researchers have investigated

* Corresponding author. Tel. +1-720-933-1211.
E-mail address: bartar@purdue.edu.

several ways to recover the expansion work. The two most common methods for expansion work recovery in VCCs are ejectors and expanders. The former has been proven to be more reliable and is by far the most common technique used in industry. Two of the most common techniques for controlling an ejector are actively-varying geometry of a single ejector [2-4] or the use of a multiple fixed-geometry ejectors in parallel [5-7]. While expanders have been theoretically shown to have greater potential for increased coefficient of performance (COP) benefits relative to ejectors, designing these devices for application in HVAC&R with a high enough isentropic efficiency to realize this gain has proven to be challenging, before even considering how to control them. To reduce overall development costs, high-fidelity VCC system models have been extensively researched as well. Both dynamic and steady-state models have been researched, but within those categories there is still a lack of charge-sensitive mechanistic models. Consideration of the charge inventory within a VCC and its optimization are essential to overall cycle performance. Experimentally-validated charge-sensitive mechanistic models utilizing charge tuning methods proposed by Shen et al. [8] have been developed by Bahman et al. for a 4-component VCC [9] as well as a VCC with economization and compressor vapor-injection [10].

This study focuses on the development of a detailed mechanistic model for an R-410A residential heat pump system that utilizes an expansion work recovery device with phase separation and an evaporator vapor bypass previously investigated by Czapla et al. [11] and Barta et al. [12]. Cycle performance was predicted with imposition of charge inventory with estimation using both one- and two-point tuning methods. Individual component efficiencies within the expander were modeled and experimentally-validated to isolate losses within the component.

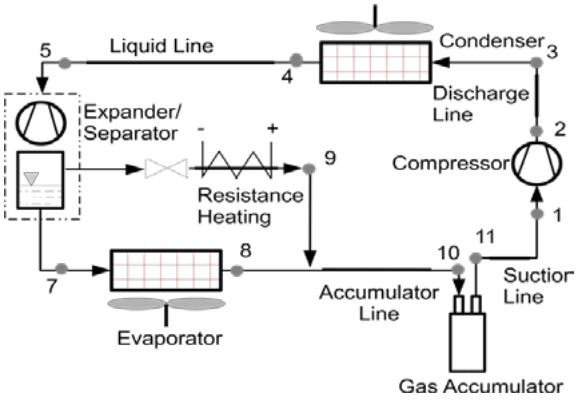

Fig. 1. Schematic of mechanistic cycle model that shows the main system components

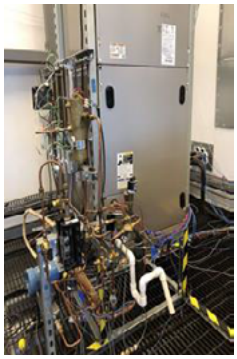

Fig. 2. View of the indoor unit showing the expander

Fig. 3. View of the variable-speed rolling piston compressor

2. Model Description

Fig. 1 shows the schematic of the variable-speed heat pump system to be modeled, with a photo of the indoor unit shown in Fig. 2. The primary difference between this cycle and a standard four-component VCC is the inclusion of the expander/separator, which simultaneously recovers expansion energy and separates vapor and liquid phases from the turbine outlet. The liquid exits the bottom of the expander housing to enter the evaporator, while the vapor exits the top before passing through a resistive heater to ensure superheat and mixing with the evaporator outlet upstream of the accumulator. The cycle components are simulated in an object-oriented fashion by using the programming language Python [13]. The thermo-physical properties of the working fluid (R-410A) were obtained from Bell et al. [14].

2.1. Compressor model

A variable speed reciprocating compressor model proposed by Mendoza-Miranda et al. [15] was used which is based on dimensionless volumetric, isentropic, and overall efficiencies. This model has also been shown to be applicable to scroll and rotary rolling piston compressors. The model characterized the compressor efficiencies in terms of certain groups of dimensionless parameters. Specific experimental data from a 5-ton (17.58 kW) Hitachi variable speed rotary rolling piston compressor (Fig. 3) were used to determine the values of the dimensionless parameters (*i.e.,* a_i coefficient values). Furthermore, the model was capable of accounting for different working fluids. In particular, Mendoza-Miranda et al. [15] employed the model to analyze the performance of a variable speed reciprocating compressor using R-1234yf, R-1234ze(E), and R-450A as alternatives to R-134a. Bahman et al. [9] validated the model for variable speed rolling-piston compressor using R-410A. The correlations for the dimensionless efficiencies were expressed as a power law function of the remaining π groups and given in Eqs. 1 to 3. The dimensionless groups for volumetric, isentropic, and overall efficiency can be found in Bahman et al. [9].

$$\eta_v = \pi_2^{0.1257}\pi_4^{0.0958}\pi_5^{0.4158} \quad (1)$$

$$\eta_s = \pi_2^{0.2166}\pi_3^{0.34781}\pi_4^{0.0773}\pi_6^{-0.03923} \quad (2)$$

$$\eta_{oa} = \pi_2^{-0.3632}\pi_3^{-0.30562}\pi_6^{0.02766}\pi_7^{0.76003} \quad (3)$$

The comparisons between measured and predicted values of the compressor mass flow rate, discharge temperature, and electric power input can be found in Bahman et al. [9].

2.2. Heat exchanger models

The heat exchanger models from Bell [16] were modified to be used in this work. The condenser model

was constructed using a moving boundary method, which divides the heat exchangers according to the phases of refrigerant flow. Each section of the heat exchanger models was simulated using the ε-NTU method as separate crossflow fin-and-tube heat exchangers with louvered fins [17], assuming constant refrigerant pressure equal to the saturation pressure.

To accurately estimate the behavior of the heat transfer from the air to the refrigerant side of the evaporator, the partially-wet and partially-dry method by Braun [18] is utilized in predicting the air side sensible and latent heat transfer when the surface temperature of the coil falls below the dew-point of air at the inlet of the evaporator. The evaporator model was solved by separating the heat exchanger into two sections. The section with surface temperatures higher than the dew-point was solved by a completely dry analysis, while the other section was solved assuming a completely wet analysis. Both heat exchanger models included Zivi slip flow model [19] to improve the refrigerant charge estimation in the two-phase region. The correlations used to estimate the heat transfer coefficients and friction factors in the condenser and evaporator models are summarized in Table 1, while the geometrical parameters used are listed in Table 2.

Both evaporator and condenser fans were modeled by using experimental data for steady-state operation conditions. The average airflow rate and power consumption for the evaporator fan were equal to 0.826 m^3/s and 0.4 kW, respectively, while the airflow across the condenser fan was equal to 1.91 m^3/s corresponding to an average measured power consumption of 0.25 kW.

Table 1. Heat transfer and pressure drop correlations in heat exchanger models

		Single-Phase	Two-Phase
Refrigerant-Side	Heat Transfer	Gnielinski [20]	Condensation: Shah [21], Evaporation: Shah [22]
	Pressure Drop	Churchill [23]	Lockhart and Martinelli [24]
Air-Side	Heat Transfer	Wang et al. [25]	
	Pressure Drop	Wang et al. [25]	
	Fin Efficiency	Schmidt [26] modified by Hong and Webb [27]	

Table 2. Geometrical parameters in heat exchanger models

Parameter	Condenser	Evaporator	Parameter	Condenser	Evaporator
Number of tubes per bank	24	60	Transverse distance of tubes [mm]	25.4	25.4
Number of banks	2	3	Fins per inch	20	14.5
Number of circuits	8	8	Fin waviness [mm]	1.0	1.0
Length of tubes [mm]	2252	452	Half-wavelength of fin wave [mm]	1.0	1.0
Outer diameter of tubes [mm]	9.13	9.13	Fin thickness [mm]	0.11	0.11
Inner diameter of tubes [mm]	8.49	8.49	Conductivity of fins [W/m-K]	237	117
Longitudinal distance of tubes [mm]	19.1	19.1			

2.3. Expander and separator model

The expander model consisted of a series of sub-models whose efficiencies were experimentally validated. A schematic showing the sub-models is provided in Fig. 4. The thermo-physical properties of the inlet state were measured, and the electrical power $\dot{W}_{elec}$ output was also measured. Generator efficiency η_{elec} was assumed to be 88% per manufacturer recommendation and mechanical efficiency η_{mech} was assumed to be 90%.

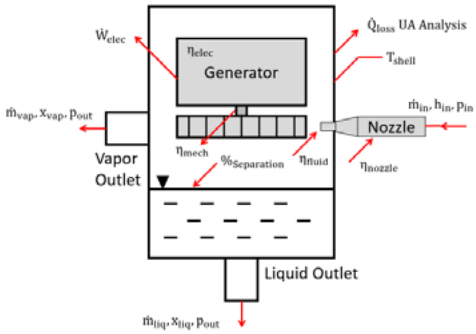

Fig. 4. Expander schematic with sub-model efficiencies

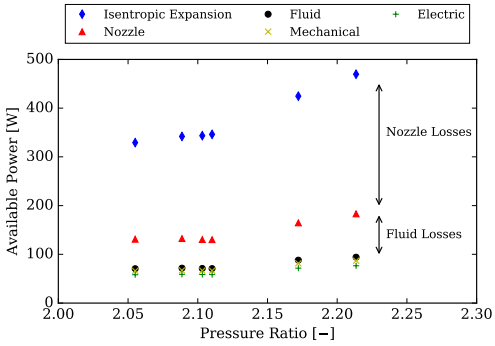

Fig. 5. Expander sub-model power availability visualization

An experimentally-validated nozzle model from Stania [28] was utilized to determine the nozzle isentropic efficiency η_{nozzle}. The nozzle model was developed for converging nozzles and includes modifications to Elliot and Weinberg [29] such as the inclusion of inter-phase drag within the vapor dome and the Smith [30] slip flow model, among others. These calculations left only the fluid efficiency, which represents losses between the outlet of the nozzle and turbine, as well as when the flow impacts the turbine. Using six experimental data points, a polynomial of this efficiency was developed as a function of expander pressure ratio. The assessed power extracted from each sub-model is shown in Fig. 5. Additionally, a natural convection heat transfer analysis was conducted to estimate the heat loss. The heat transfer rates were on the order of 2 to 5 W, but this transfer was important for completeness of the energy balance. Finally, ideal separation of phases was not achieved experimentally. As such, the liquid outlet quality was estimated as 0.025 from experimental data.

2.4. Linesets model

The pressure drop of refrigerant flow in the system linesets was calculated using ACHP model Bell [31] with the Churchill [23] correlation to estimate the pressure drop friction factor. The ε-NTU method from Bergman et al. [17] was used to estimate the amount of heat loss, if any, in all the linesets. Note that the volume of the linesets was considered for the purpose of refrigerant charge calculation. The geometry of the pipelines was measured from the experimental setup and is summarized in Table 3.

Table 3. Geometrical parameters of the system linesets

	Suction line	Discharge line	Liquid line	Accumulator line

Length [mm]	7600	300	7600	571
Outer diameter of tubes [mm]	28.58	28.58	9.53	22.23
Inner diameter of tubes [mm]	26.04	26.04	6.35	19.05
Insulation thickness [mm]	20	-	20	-
Conductivity of tubes [W/m-K]	0.19	0.19	0.19	0.19
Conductivity of insulation [W/m-K]	0.036	-	0.036	-

2.5. Accumulator model

A suction gas accumulator was modeled as a cylindrical vapor-only container. This implies that natural heat transfer occurred between the surfaces of the accumulator and the surroundings. The natural convection correlations from Bergman et al. [17] was used to account for the heat transfer across the circumference of the accumulator. The volume of the accumulator was considered for the purpose of refrigerant charge estimation. The accumulator has a height of 274 mm with inner and outer diameters of 115 mm and 123.6 mm, respectively.

2.6. Charge model

Due to the inaccurate estimation of the system volumes, ambiguous flow patterns under two-phase flow conditions, and amount of refrigerant dissolved in the compressor lubricant, both a single-point and a two-point charge tuning procedure were implemented based on the methodology proposed and validated by Shen et al. [8]. The total refrigerant charge of the system is given by the sum of the mass calculated by the cycle model and a contribution fitted onto the experimental data, which can be expressed as

$$m_{\text{charge}} = m_{\text{pred}} + \Delta m_{\text{liq}} \tag{4}$$

$$\Delta m_{\text{liq}} = C + K\left(w_{\text{liq,pred}} - w_{\text{ref}}\right) \tag{5}$$

where C, K, and w_{ref} are the coefficients to be determined through only two experimental data points to calibrate the model. The tuning coefficients are listed in Table 4. Note that for the one-point regression model, Eq. 5 results with the coefficient C only.

Table 4. Charge model tuning coefficients

C [kg]	0.987
K	-1.059
w_{ref}	0.0466

2.7. Pre-conditioner model

In order to obtain good initial guesses and reduce computational time for the main cycle solver, a pre-conditioner model from Bell [31] was modified to estimate values for refrigerant evaporation and condensation temperatures. The pre-conditioner model duplicates the main cycle to be solved with simplified models for condenser and evaporator, as shown in Fig. 6. The independent variables (*i.e.,* T_{evap} and T_{cond}) are iterated to minimize the residual vector (Eq. 6) by means of *fsolve* function [32] until convergence. Note that the superheat degree T_{sh} is deterministically evaluated in the main cycle. However, in the pre-conditioner model a targeted value was used as an input to ensure continuity.

$$\vec{\Delta} = \begin{bmatrix} \dot{W}_{\text{comp}} + \dot{Q}_{\text{evap}} - \dot{Q}_{\text{cond}} - \dot{W}_{\text{exp}} + \dot{Q}_{\text{heater}} \\ \dot{Q}_{\text{cond,a}} - \dot{Q}_{\text{cond,r}} \\ \dot{Q}_{\text{evap,a}} - \dot{Q}_{\text{econ,r}} \end{bmatrix} \tag{6}$$

2.8. Overall system model

The flow chart in Fig. 7 shows the algorithm used in the system-level solver. The components in the system-level model were simulated consecutively as shown in Fig. 7. The independent variables (*i.e.,* T_{evap}, T_{cond}, and T_{sh}) are iterated by means of the Broyden [33] method to drive the residual vector (Eq. 7) to zero.

$$\vec{\Delta} = \begin{bmatrix} m_{charge} - m_{charge,target} \\ h_{mix,out} - h_{accum.in} \\ \dot{Q}_{heater} - \dot{Q}_{target} \end{bmatrix} \tag{7}$$

The model checks for the pressure drop residual (Eq. 8) after the residual vector (Eq. 7) converges. The pressure drops in the high- and low-pressure linesets are considered after the cycle iteration completed to avoid numerical difficulties. Hence, new effective saturation temperatures (*i.e.,* T^*_{cond} and T^*_{evap}) are calculated and iterated in the cycle model until the updated effective pressure drops (*i.e.,* P^*_{high} and P^*_{low}) are equal to the pressure drop terms calculated from the converged cycle model (*i.e.,* P_{high} and P_{low}). The solver converges when the pressure drop residual (Eq. 8) is less than 1 Pa.

$$\vec{\Delta} = \begin{bmatrix} P^*_{high} - P_{high} \\ P^*_{low} - P_{low} \end{bmatrix} \tag{8}$$

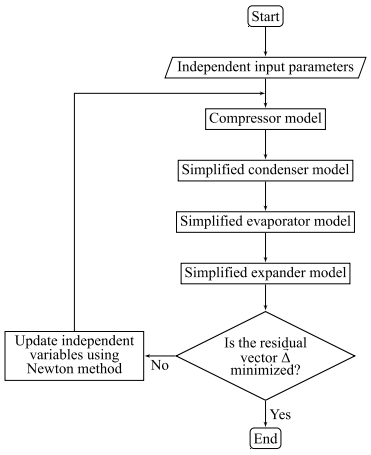

Fig. 6. Flowchart of pre-conditioner solver

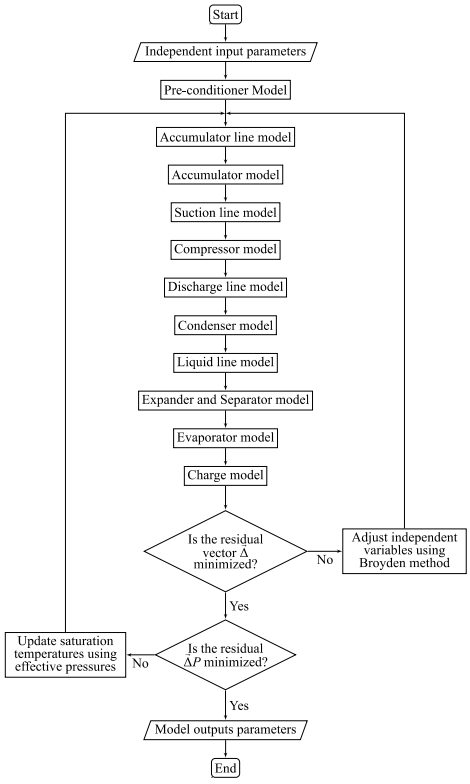

Fig. 7. Flowchart of mechanistic cycle solver

Table 5. Testing conditions for heat pump system with expander

Test	Outdoor condition		Indoor condition	
	Dry-bulb [°C]	Wet-bulb [°C]	Dry-bulb [°C]	Wet-bulb [°C]
1	35.1	23.3	25	17.7
2	40.0	27.3	25.1	17.8
3	42.0	28.9	25	17.7
4	35.0	23.4	26.8	19.2
5	35.0	23.4	23.5	16.5
6	35.0	23.4	24.0	16.9

3. Results and Discussion

3.1. Experimental methodologies

A 5-ton (17.58 kW) single-stage split-type heat pump with R-410A as the working fluid was installed inside a pair of psychrometric chambers at the Herrick Laboratories. A variable-speed rolling piston compressor was installed to replace the original scroll compressor, and the expander device was installed to replace the original TXV. The unit was tested at six points according to the test matrix in Table 5. All test conditions were performed according to AHRI Standard 210/240 [34] conditions using refrigerant-side data. The unit was charged with 4.81 kg (10.6 lb) to ensure consistent subcooling in the liquid line. Experimental cooling capacity, $\dot{Q}_{\text{evap}}$, and COP values for these test conditions are provided in Fig. 8. Cooling capacity and COP were defined based on AHRI Standard 210/240 [34] as shown in Eq. 9 and Eq. 10, respectively.

$$\dot{Q}_{\text{evap}} = \dot{m}_{\text{ref}}\left(h_{\text{evap,out}} - h_{\text{evap,in}}\right) \tag{9}$$

$$\text{COP} = \frac{\dot{Q}_{\text{evap}}}{\dot{W}_{\text{tot}}} \tag{10}$$

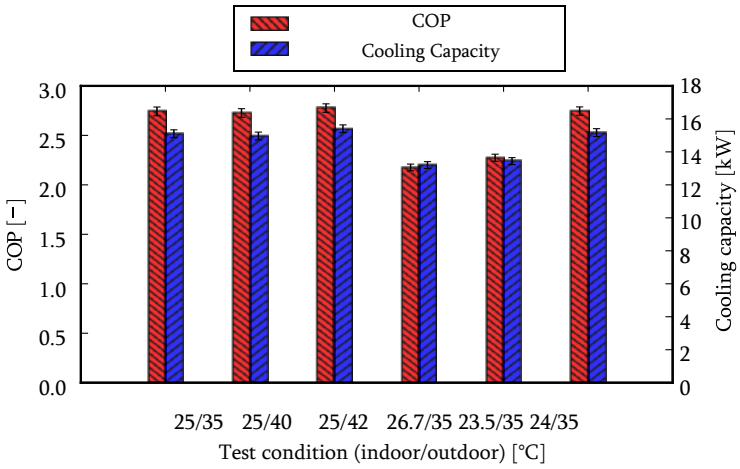

Fig. 8. Experimental COP and cooling capacities

Table 6. Tuning multipliers for expander heat pump cycle model

Compressor displacement scale factor	1.002
Condenser air-side convection heat transfer coefficient	1.289
Condenser refrigerant-side convection coefficient	0.973
Condenser refrigerant-side pressure drop correlation	1.077
Evaporator air-side convection heat transfer coefficient	1.302
Evaporator refrigerant-side convection coefficient	1.6
Evaporator refrigerant-side pressure drop correlation	0.998
Expander and separator vapor mass fraction	0.058

3.2. Model tuning

There was a systematic bias between the simulation and experimental results due to simplifications and imperfect information related to the heat pump system components. To minimize the bias, eight tuning multipliers were introduced to adjust mass flow rates, heat transfer coefficients and pressure drop on both air-side and refrigerant-side for the condenser and evaporator model as well as the separation fraction in the expander. The estimation of the multipliers was conducted by means of an iterative scheme to eliminate the discrepancy between the experimental results and the estimations of the mass flow rates, the condenser and evaporator heat transfer rates, the compressor power consumption, and the expander power generation. The optimization problem was solved with a bounded differential evolutionary (DE) method [35] and the resulting tuning factors are summarized in Table 6. It can be noticed from Table 6 that the air-side multipliers for the evaporator and the condenser are relatively high (approximately equal to 1.3) due to the influence of the air leakage around the heat exchangers in the experimental measurements.

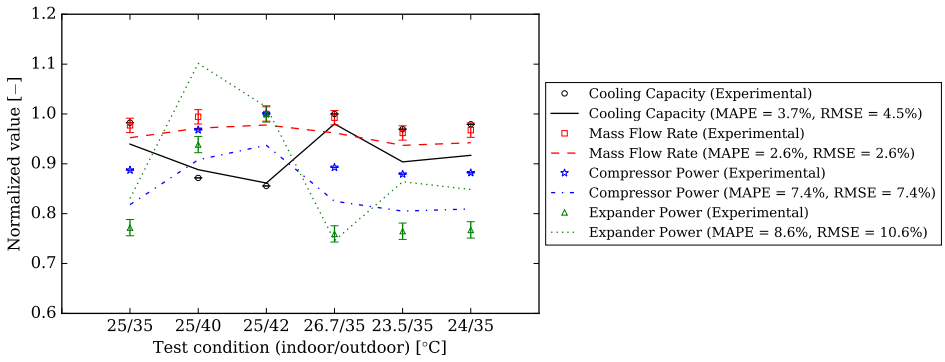

Fig. 9. Comparison of estimated model performance parameters with experimental data (normalized with maximum experimental value)

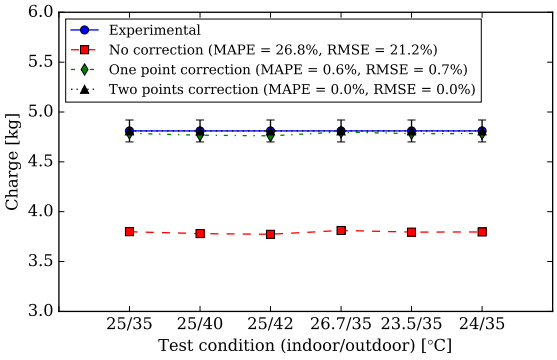

Fig. 10. Comparison of charge prediction with experimental data using one- and two-point regression charge model

3.3. Model validation

The validation was carried out with the six test conditions which were experimentally conducted on the retrofitted heat pump unit with expander device and variable-speed rolling piston compressor. The comparisons of the refrigerant mass flow rate, the condenser and evaporator capacities as well as the compressor power consumption and expander power generation between the model simulations and the experimental results are illustrated in Fig. 9. The error between the predicted and experimental values is calculated by the mean absolute percentage error (MAPE) and the root mean square deviation error (RMSE). Fig. 9 shows that the model, after tuning, captured the system and component performances within a reasonable margin of error. The minimum MAPE and RMSE of 2.6% and 2.6% corresponded to the total mass flow rate, while the maximum MAPE and RMSE of 8.6% and 10.6% were associated with the predictions of the expander power generation, respectively.

Using the charge model coefficients (Table 4) and the system tuning factors (Table 6), as well as by imposing the system charge inventory, the cycle was simulated at the same experimental test conditions to assess the charge estimation as shown in Fig. 10. Fig. 10 compares the charge predictions for the cases without any correction with one-point regression charge model, and with two-point model. It can be seen that the one-point charge model eliminates all the biases and predicts the charge inventory with MAPE and RMSE less than approximately 1%, while the two-point charge model [8] perfectly estimates the system charge with no errors.

4. Conclusions and Recommendations

This paper aimed to develop a detailed mechanistic and charge-sensitive model for an expander heat pump system to accurately estimate the system performance. The developed system model was tuned and validated with experimental data from a 5-ton (17.58 kW) single-stage split-type heat pump tested at different operating conditions in the Herrick Laboratories. The results yielded the following conclusions. First, the mechanistic expander heat pump system model predicted the performance parameters (*i.e.,* mass flow rates, compressor and expander power, and heat exchanger capacities) with a reasonable margin of MAPE and RMSE less than approximately 9% and 11%, respectively. Second, the charge imposed model with one- and two-point correction methods accounted for the discrepancy in refrigerant charge estimation with MAPE and RMSE less than approximately 1%. Finally, the detailed charge inventory model allows the analyses of drop-in working fluid replacements and their effects on the system sizing. Furthermore, the model also allows to optimize the charge level to take advantage of variable-speed compressors and power generation expanders. Future work entails the use of the system model for system, charge, drop-in fluid assessment, and multi-objective economic optimization. Additionally, the sub-models will be utilized to prioritize expander component re-design and further experimental analysis.

Acknowledgements

The authors would like to acknowledge the support from the Center for High Performance Buildings (CHPB) at the Ray W. Herrick Laboratories as well as the Research Section at Kuwait University for the financial and technical support.

References

[1] USEIA. U.S. Energy Information Agency Monthly Energy Review - April 2018. 2018.
[2] Elbel, S., Hrnjak, P. Experimental validation of a prototype ejector designed to reduce throttling losses encountered in transcritical R744 system operation. *Int. J. Refrig.* 2008;**31(3)**:411–422.
[3] Carel. EmJ - Carel electronic modulating ejector. Carel.com. 2019.
[4] Bodys, J., Smolka, J., Palacz, M., Haida, M., Banasiak, K., Nowak, A., Hafner, A. Performance of fixed geometry ejectors with a swirl motion installed in a multi-ejector module of a CO2 refrigeration system. *Energy*. 2016;**117**:620-631.
[5] Hafner, A., Försterling, S., Banasiak, K.. Multi-ejector concept for R-744 supermarket refrigeration. *Int. J. Refrig. 2014;***43**:1–13.
[6] Hafner, A., Schönenberger, J., Banasiak, K., Girotto, S., 2014. "R744 ejector supported parallel vapour compression system," Proc. of the 3rd IIR International Conference on Sustainability and Cold Chain. London, UK. p. 23–25.
[7] Pardiñas, Á. Á., Hafner, A., Banasiak, K. Novel integrated CO2 vapour compression racks for supermarkets. Thermodynamic analysis of possible system configurations and influence of operational conditions. *Appl. Therm. Eng.* 2018;**131**:1008–1025.
[8] Shen, B., Braun, J. E., Groll, E. A. Improved methodologies for simulating unitary air conditioners at off-design conditions. *Int. J. Refrig.* 2009;**32(7)**:1837–1849.
[9] Bahman, A. M., Ziviani, D., Groll, E. A., 2018. "Development and validation of a mechanistic vapor-compression cycle model," Proc. of the 17th Int. Refrig. and Air Cond. Conf. at Purdue. West Lafayette, Indiana, USA. Paper #2444.
[10] Bahman, A. M., Ziviani, D., Groll, E. A., 2018. "Validation of a charge-sensitive vapor-injected compression cycle model with economization," Proc. of the 17th Int. Refrig. and Air Cond. Conf. at Purdue. West Lafayette, Indiana, USA, Paper #2445.
[11] Czapla, N., Inamdar, H., Salts, N., Groll, E. A., 2016. “Performance testing of unitary split-system heat pump with an energy recovery expansion device,” Proc. of the 16th Int. Refrig. and Air Cond. Conf. at Purdue. West Lafayette, Indiana, USA. Paper #2549.
[12] Barta, R. B., Simon, F., Groll, E. A., 2018. “Experimental analysis and design improvements on combined viper expansion work recovery turbine and flow phase separation device applied in R410A heat pump,” Proc. of the 17th Int. Refrig. and Air Cond. Conf. at Purdue. West Lafayette, Indiana, USA. Paper #2251.
[13] Python, “Python Language Reference, Version 2.7.13,” 2016.
[14] Bell, I. H., Wronski, J., Quoilin, S., Lemort, V. Pure and pseudo-pure fluid thermophysical property evaluation and the open-source thermophysical property library CoolProp. *Ind. Eng. Chem. Res.* 2014;**53(6)**:2498–2508.
[15] Mendoza-Miranda, J. M., Mota-Babiloni, A., Ramírez-Minguela, J. J., Munoz-Carpio, V. D., Carrera-Rodriguez, M., Navarro-Esbri, J., Salazar-Hernandez, C. Comparative evaluation of R1234yf , R1234ze (E) and R450A as alternatives to R134a in a variable speed reciprocating compressor. *Energy*. 2016;**114**:753-766.
[16] Bell, I. H., Quoilin, S., Georges, E., Braun, J. E., Groll, E. A., Hortung, W. T., Lemort, V. A generalized moving-boundary algorithm to predict the heat transfer rate of counterflow heat exchangers for any phase configuration. *Appl. Therm. Eng.* 2015;**79**:192–201.
[17] Bergman, T. L., Incropera, F. P., DeWitt, D. P., Lavine, A. S. *Fundamentals of heat and mass transfer, 7th edition*, John Wiley & Sons; 2011.
[18] Braun, J. E., 1988. “Methodologies for the Design and Control of Central Cooling Plants,” PhD Thesis.
[19] Zivi, S. M. Estimation of steady-state steam void-fraction by means of the principle of minimum entropy production. *J. Heat Transf.* 1964;**86(2)**:247-251.
[20] Gnielinski, V. New equations for heat and mass transfer in turbulent pipe and channel flow. *Int. Chem. Eng.* 1976;**16(2):**359–368:.
[21] Shah, M. M. A general correlation for heat transfer during film condensation inside pipes. *Int. J. Heat Mass Transf.* 1979;**22(4):**547–556.
[22] Shah, M. M. A new correlation for heat transfer during boiling flow through pipes. *ASHRAE Trans.* 1976;**82**:66–86.

[23] Churchill, S. W. Friction-factor equation spans all fluid-flow regimes. *Chem. Eng.* 1976;**84(24)**:91–92.
[24] Lockhart, R., Martinelli, R. Proposed correlation of data for isothermal two-phase, two-component flow in pipes. *Chem. Eng. Prog.* 1949;**45(1)**:39–48.
[25] Wang, C. C., Tsai, Y. -M., Lu, D. -C. Comprehensive study of convex-louver and wavy fin-and-tube heat exchangers. *J. Thermophys. Heat Transf.* 1998;**12(3)**:423–430.
[26] Schmidt, T. E. La production calorifique des surfaces munies d'ailettes. *Annex. Du Bull. L'Institut Int. Du Froid, Annex* 1945;**G-5**.
[27] Hong, K. T., Webb, R. L. Calculation of fin efficiency for wet and dry fins. *HVAC&R Res.* 1996;**2(1)**:27–41.
[28] Stania, L., 2019. "Experimental Analysis of a Viper Expansion Turbine for Work Recovery and its Factors Influencing Cycle Stability within a R410A Residential Heat Pump," Ray W. Herrick Labs Final Report.
[29] Elliott, D. G., Weinberg, E., 1968. "Acceleration of liquids in two-phase nozzles," Jet Propuls. Lab., Tech. Rep. 32-987.
[30] Smith, S. L., 1969, "Void fractions in two-phase flow: A correlation based upon an equal velocity head model," Proc. Inst. Mech. Eng. **184(1)**, p. 647–664.
[31] Bell, I. H., "Air conditioning and heat pump mpdel (ACHP) source code version 1.5," 2015.
[32] More, J., Garbow, B., Hillstrom, K., "User guide for MINPACK-1," 1980.
[33] Broyden, C. G. A class of methods for solving nonlinear simultaneous equations. *Math. Comput.* 1965;**19(92)**:577–593.
[34] ANSI/AHRI, "Performance rating of unitary A/C and air-source heat pump equipment 210/240," 2008.
[35] Storn, R., Price, K. Differential evolution - a simple and efficient heuristic for global optimization over continuous spaces. *J. Glob. Optim.* 1997;**11(4)**:341–359.

Nomenclature

A	Dimensionless coefficient	-
C	Charge tuning coefficient	kg
h	Specific enthalpy	$\frac{kJ}{kg}$
K	Charge tuning coefficient	-
k	Thermal conductivity	$\frac{W}{m-K}$
L	Length	mm
m	Mass	kg
M	Molar mass	$\frac{kg}{kmol}$
$\dot{m}$	Mass flow rate	$\frac{kg}{s}$
N	Speed	$\frac{1}{min}$
P	Pressure	kPa
$\dot{Q}$	Heat transfer rate	kW
T	Temperature	°C
UA	Overall heat transfer	$\frac{W}{K}$
V	Volume	m^3
$\dot{V}$	Volumetric flow rate	$\frac{m^3}{s}$
W	Charge tuning coefficient	-
$\dot{W}$	Power	kW
X	Quality	-

Greek Symbols

Δ	Change	-
$\vec{\Delta}$	Residual vector	Multiple

Acronyms

ACHP	Air Conditioning Heat Pump Software
COP	Coefficient of Performance
DE	Differential Evolutionary
EXV	Electronic Expansion Valve
HVAC&R	Heating, Ventilation, Air Conditioning and Refrigeration
MAPE	Mean Absolute Percentage Error
NTU	Number of Transfer Unit
RMSE	Root Mean Square Deviation Error
TXV	Thermostatic Expansion Valve
VCC	Vapor-Compression Cycle

Subscript

a	Air
accum	Accumulator
amb	Ambient
comp	Compressor
cond	Condenser
dis	Discharge
disp	Displacement
elec	Electric
evap	Evaporator
exp	Expander

ε	Effectiveness	-	gen	Generator
η	Efficiency	-	I	Coefficient
π	Dimensionless coefficient	-	liq	Liquid
ρ	Density	$\frac{kg}{m^3}$	mech	Mechanical
			oa	Overall isentropic
			pred	Predicted
			R	Refrigerant
			ref	Reference
			S	Isentropic
			suc	Suction
			sh	Superheat
			V	Volumetric
			*	Effective